ROMANIAN JOURNAL OF INFORMATION SCIENCE AND TECHNOLOGY
Volume **13**, Number 4, 2010, 378–388

On Designing a Positioning and Detection System for a Lab-on-a-Chip Device

Marius VOLMER[1,2], Marioara AVRAM[2]

[1] *Transilvania* University of Braşov, Eroilor 29, Braşov, Romania
E-mail: volmerm@unitbv.ro

[2]National Institute for Research and Development in Microtechnologies, Str. Erou Iancu Nicolae 126A, Bucharest, Romania
E-mail: marioara.avram@imt.ro

Abstract. The manipulation and detection of magnetic carriers used for biosensing represent key features in a lab-on-a-chip (LOC) device. In this contribution we present some results regarding the analysis of a manipulation system and the interaction between the magnetic nanoparticles (MNPs) and the spin valve sensor used for detection. We found that the detection sensitivity is strongly related with the position of the magnetic particles on the sensor's surface. A net signal can be obtained for a single magnetic nanoparticle of 100 nm in diameter. For micromagnetic simulations the employed program was SimulMag.

Key words: Biomedical application; Lab-on-chip; Magnetic nanoparticles; Giant magnetoresistance, Planar Hall effect sensors; Micromagnetic simulations.

1. Introduction

Recent development in MEMS (microelectromechanical systems) has brought a new tool in biological or chemical applications: "lab-on-a-chip" (LOC). New terminology, such as micro total analysis systems (μTAS) and lab-on-a-chip was introduced in the last decade and several prototype systems have been reported. The idea of lab-on-a-chip is basically to reduce biological or chemical laboratories to a microscale system, hand-held size or smaller.

Lab-on-a-chip systems can be made out of silicon, glass, and polymeric materials, and the typical microfluidic channel dimensions are in the range of several tens to hundreds of μm. Liquid samples or reagents can be transported through the

microchannels from reservoirs to reactors using electrokinetic, magnetic, or hydrodynamic pumping methods. Fluidic motions or biochemical reactions can also be monitored using various sensors.

One of the most important advantage of LOC devices lies in their low cost. Another advantage is that lab-on-a-chip requires very small amounts of reagents/chemicals (which enables rapid mixing and reaction) because biochemical reaction is mainly involved in the diffusion of two chemical or biological reagents, and microscale fluidics reduces diffusion time as it increases reaction probabilities. In practical terms, reaction products can be produced in a matter of seconds/minutes, whereas laboratory scale can take hours, or even days. In addition, lab-on-a-chip systems can be portable devices.

Complex reactions of many reagents could happen on lab-on-a-chip that have ultimate potential in DNA analysis, biochemical warfare agent detection, biological cell/molecule sorting, blood analysis, drug screening/development, combinatorial chemistry, and protein analysis. Two recent developments of microfluidic systems for lab-on-a-chip applications are to be mentioned: (i) magnetic micro/nano bead-based biochemical detection system and (b) disposable smart lab-on-a-chip for blood analysis.

Besides the flowing of biological fluids inside the LOC microchanels, it is also possible to manipulate them on-chip, as demonstrated in the following. This is important for actuation process and precisely positioning [1] of biological molecules over the sensor region.

Detection of the fields generated by magnetic beads which are used to label chemical or biological species of interest can be made using giant magnetoresistive (GMR), magnetic tunnel junctions (MTJ) or Planar Hall effect (PHE) spin-valve structures [2–7]. The magnetic beads polarized by a DC or AC magnetic field can affect the magnetization state of the spin-valve sensor, leading to a detectable signal. Results from theoretical modelling, as well as laboratory tests, show that spin-valve sensors can resolve single micrometer-sized magnetic beads [5–7]. Because both systems, microbeads and spin-valve sensors, are made-up from magnetic materials, there is a magnetostatic interaction between them that causes changes of the magnetisation curves of the beads and sensor which in turns decide the magnetoelectric behaviour of the sensor. The external magnetic field can be applied either parallel or perpendicular to the sensor surface. Because the value of the demagnetising field over a direction perpendicular to the film surface is so large, the spin-valve devices are sensitive only for in plane magnetic fields. Therefore, it is possible to apply a rather large magnetizing field in the out-of-plane orientation of the magnetoresistive sensor without directly affecting the sensor itself [7]. On the other hand, the microbeads placed under the action of this field will be magnetised and can generate in-plane magnetic fields that, in turn, will magnetise the sensor. So, even for an out-of-plane magnetic field, a GMR response can be obtained. Applying the magnetizing field in the plane of the sensor requires magnetoresistive devices with sensitive regions at rather large in-plane fields or ferromagnetic markers with large magnetic moment. Otherwise, the magnetic moment of the superparamagnetic microspheres is insufficient to produce measurable stray fields. For this reasons, we found that the best setup when using

GMR sensors is to apply the field in the out-of-plane direction, perpendicular to the sensor surface [8]. The microsphere's magnetic moment can be zero, or can be different from zero by varying the magnitude of the magnetizing field in the out-of-plane setup without directly affecting the magnetoresistive sensor itself. Thus, in this setup, the same sensor element can also act as a reference.

A micromagnetic simulator, SimulMag [9], was used to generate the positioning system, the sensor structure and to analyse the behaviour of these systems and their interaction with the superparamagnetic beads (sppm).

2. Results and discussion

In what follows will be presented some results regarding the detection of sppm beads by spin-valve sensors and then our simulations on manipulation of molecules by magnetic carriers using a simple electrical circuit.

2.1. Detection by magnetoresistive sensors

The simulated GMR sensor is an exchange-biased spin-valve structure 1×1 μm^2 of the type FeMn/$Ni_{80}Fe_{20}$(10 nm)/Cu(4 nm)/$Ni_{80}Fe_{20}$(10 nm). The sppm microbeads are placed on sensor' surface as shown in Fig. 1. The thickness of the immobilization and protection layer (Si_3N_4) between the beads and the GMR sensor is 0.2 μm. Each bead is assumed to be a superparamagnetic sphere of magnetite with a diameter of about 0.2 μm and a saturation magnetization of about 110 kA/m (or 110 emu/cm^3) as can be derived from [3, 7]. The most part of this value is obtained for a field of about 500 Oe (40 kA/m) [3]. The structure used in our simulations, Fig. 1, consists from two groups: the sensor and the superparamagnetic beads. For each group the program can return, during the simulation, information regarding the field behaviour of magnetization and GMR effect [8, 9]. The field is applied perpendicular to the sensor surface, as is shown in Fig. 1b.

Each magnetic layer from this region was divided into 10×10 single domains of $Ni_{80}Fe_{20}$, 10 nm thick and 95 nm each side. The distance between the adjacent domains is $d = 5$ nm which is equivalent with an inter-grain spacing [10]. The cell size used to build the mesh is higher than usual but this is rather a phenomenological model, inspired from the film structure, as we showed on [10]. This approach was used to describe the magnetization curves, GMR and planar Hall effect in such structures and the agreement with experimental data was very good [10, 11]. The saturation magnetization of the $Ni_{80}Fe_{20}$ layers was set to 800 emu/cm^3 (800 kA/m) and the pinning field provided by the FeMn layer to the $Ni_{80}Fe_{20}$(10 nm) layer was set at $H_{pin} = 200$ Oe (15.9 kA/m) [12]. A linear analog signal is desired from the spin valve sensors for quantitative biodetection. For this purpose, the spin valve sensor is best configured in an orthogonal magnetization state [13]. The uniaxial anisotropy field was set perpendicular to the pinning field and the value was fixed at $H_K = 5$ Oe (0.39 kA/m) which is a common value for Permalloy layers. Between the two magnetic layers there is a 4 nm Cu spacer and the coupling field is set to vary periodically

between 30 and 60 Oe because of the Néel magnetostatic coupling [10]. The arrows which have the same orientations (red arrows) are from the pinned layer whereas the arrows from the free layer (the blue ones) have different orientations, Fig. 1a, in order to minimise the energy of the magnetic system (GMR sensor and magnetic beads). In Fig. 1a, the beads are placed above the centre of the free layer at a distance of 200 nm from his surface. The sppm beads are equally spaced between them. In our simulations the distance between the nearest beads is 200 nm. In order to minimize the hysteresis effects, the in plane component of magnetic field produced by the beads has to be applied perpendicular to the easy axis [13].

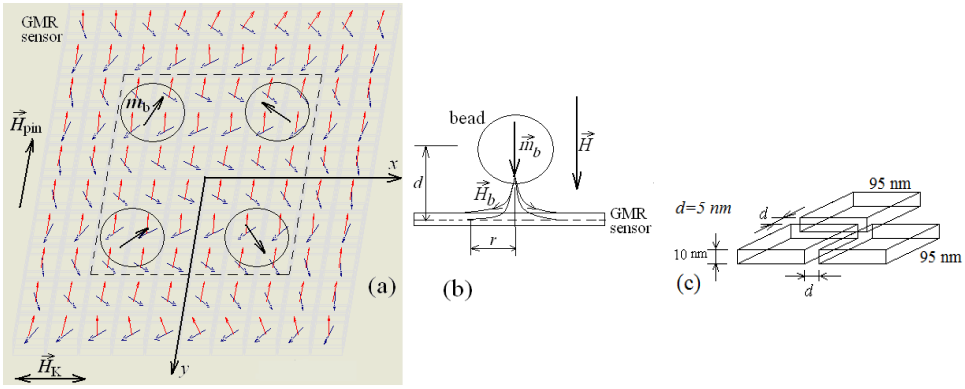

Fig. 1. (a) The structure of the spin-valve sensor used for micromagnetic simulations and the magnetic particles located above the free layer. The orientations of the anisotropy, H_K, and pinning fields, H_{pin}, are presented; m_b denotes the magnetic moment of the bead; (b) the illustration of the stray fields produced by the beads under the action of an external magnetic field; (c) detailed structure of the mesh.

The magnetic behaviour of the microbeads was simulated, in the frame of Stoner-Wohlfahrt theory, using the SimulMag program. The results are presented in Fig. 2 and emphasis the role of the particles agglomeration and the coupling effect between the grains and the spin-valve structure.

Because of the high value of the demagnetizing coefficient along the direction perpendicular to the sensor surface, the magnetic moments remain in the film plane and the magnetization curve shows a line with a very small slope. The GMR effect presents a weak field dependence and can be taken as a baseline, Fig. 3 [8]. When magnetic beads are located over the sensor, like in Fig. 1, the horizontal component of the stray field, generated by them, can change the magnetic state of the sensor and hence can produce a GMR effect. However, for a large number of particles, located over the centre of the sensor, $\Delta y = 0$, the horizontal components of the stray fields will cancel each other beneath the grains and the GMR response will be weak as we can see in Fig. 3.

If the ensemble of particles, as sketched in Fig. 1a, is moved from the centre toward the margin of the sensor, following the y direction, the horizontal components

of the stray fields, generated inside the magnetic layers by the beads, will not cancel entirely and increase the net field applied in the film plane. A GMR response will appear as we can see in Fig. 3, for some displacements, $\Delta y = 100$, 300, 500, 800 and 1000 nm, of the microbeads ensemble relative to the sensor centre. In the geometry presented in Fig. 1a, a large part of the horizontal components of the stray fields will be directed perpendicular to the easy axis of magnetization and will produce a smooth variation of the GMR effect which is useful for quantitative measurements.

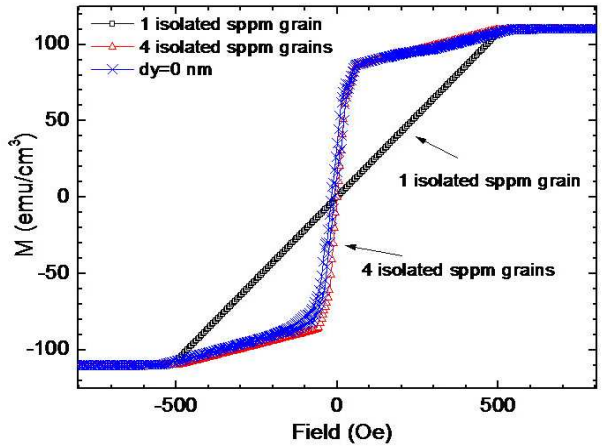

Fig. 2. The magnetization curves of 1 and 4 magnetic beads isolated and located over the sensor centre (denoted with $\Delta y = 0$).

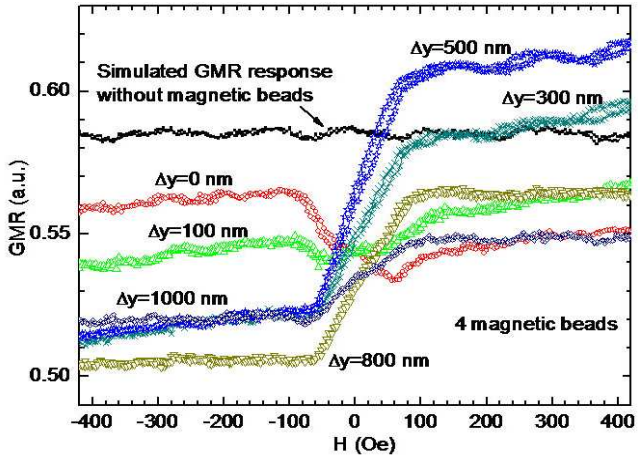

Fig. 3. Micromagnetic simulations of the GMR effect without magnetic beads over the sensor and when 4 sppm beads are located at various positions described by $\Delta y = 0$, 100, 300, 500, 800 and 1000 nm; the field is applied perpendicular to the film surface.

For the optimum position, which is around $\Delta y = 500$ nm in this model, we can plot, Fig. 4a, the field dependence of the differential output signal, *i.e.* GMR variation with magnetic beads from which is extracted the reference signal provided by an identical reference sensor (without beads), or simply the baseline obtained from the same sensor as illustrated in Fig. 3.

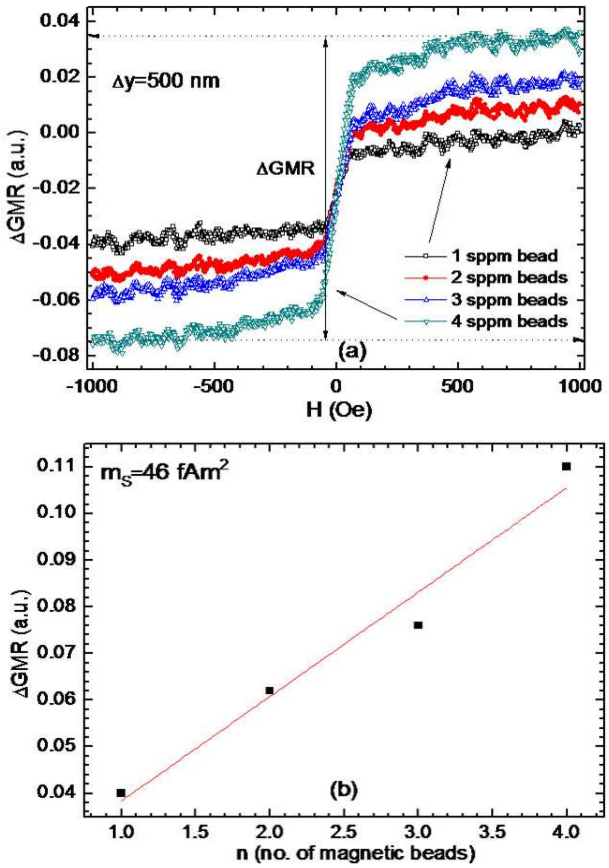

Fig. 4. (a) The field dependence of the output signal, ΔU, in function of the number of magnetic beads located over the sensor and (b) the output signal ΔU_S in function of the magnetic moments calculated from the signals at saturation. The field is applied perpendicular to the film surface.

Taking the above specified data, we can estimate a value of the magnetic moment at saturation, $m_S = 46$ fAm^2/magnetic bead and obtain a response curve of the differential sensor output in function of the beads number, Fig. 4b. It is natural to assume a small number of magnetic particles located over a surface of 1 μm^2 of the sensor. The results of these micromagnetic simulations can be extended to larger regions.

2.2. Detection by Planar Hall Effect sensors (PHE)

Although the signal derived from the PHE is small, theoretically, there is a higher signal-to-noise ratio (S/N) and a better thermal stability when compared to GMR spin valve sensors, hence it has the potential of detecting single micro- or nanoparticle [6, 7]. The planar Hall voltage depends on the magnetization quadratically at the small applied fields and parabolically at the applied fields above the saturated magnetization. Currently, the PHE related to the rotation of the magnetization is known as the anisotropic magnetoresistance (AMR) effect of the magnetic materials. If the magnetization is initially oriented along the driving current inside the sensor, a rotation with angle θ produces a PHE voltage of the form:

$$U_H = CM^2 j \cdot \sin 2\theta, \tag{1}$$

where C is a constant determined by the film geometry and material properties, j is the current density, M is the saturation magnetization and θ is the angle between the current and the magnetization vector that, in turn, is determined by the value and direction of the external magnetic field.

This property can be used to build magnetic sensors. In order to obtain a coherent rotation of the magnetization inside the PHE sensor under the action of an applied magnetic field, a magnetic biased system is proposed, Fig. 5.

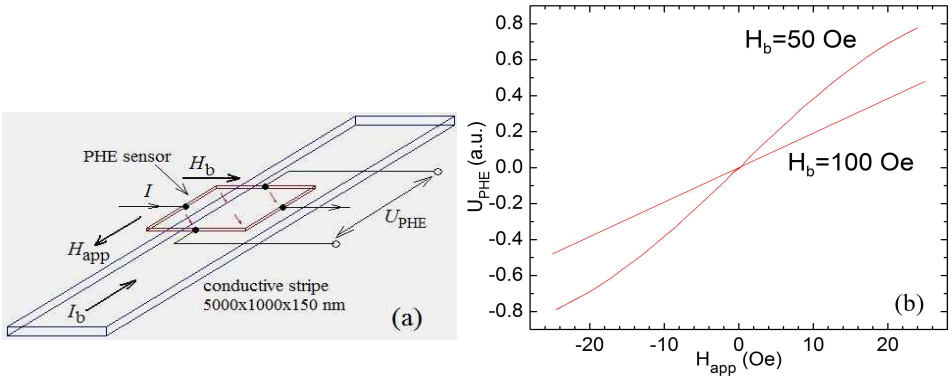

Fig. 5. (a) The setup used for biasing the sensor as designed in SimulMag. The conductive stripe is made from Cu and the sensor is a single domain of Permalloy 10 nm thick, 1 μm each side, placed at 200 nm above the stripe; (b) Results of the micromagnetic simulations for field dependence of the PHE voltage in the approximation of a single domain structure for two biasing fields. For I_b = 10.5 mA, the mean field in which is placed the sample is 100 Oe.

The current that is flowing through the conductive stripe generates a biasing magnetic field, $H_b \sim I_b$, which induces a single domain structure inside the sensor. Here, the PHE sensor consist from a thin film of Permalloy, 10 nm thick and 1 μm each side. Applying a magnetic field, H_{app}, over a direction perpendicular on H_b, will produce a rotation of the magnetization and a voltage will appear in a Hall effect setup,

Fig. 5a and b. We have to mention that for thin films of Permalloy, if $H_b < 50$ Oe, the magnetic structure is not a single domain one and the field dependence of the PHE voltage is distorted and affected by domain wall motion processes. For $H_b > 50$ Oe, the application of H_{app} produces a rotation of magnetisation with an angle θ which depends on the ratio between H_{app} and H_b. Figure 6 presents field dependences of PHE voltage measured for a disk shape multilayer structure (5 mm diameter) of the type Co/Cu/NiFe used in a setup as described above, Fig. 5a.

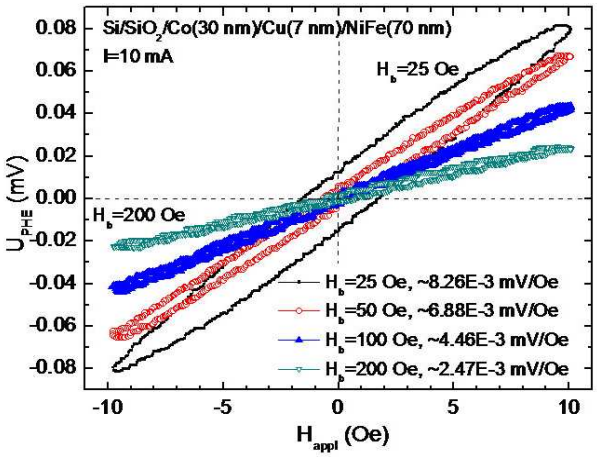

Fig. 6. Field dependences of the PHE voltage for a ML of Co/Cu/NiFe.

These measurements show hysteresis effects for low biasing fields and confirm this mechanism of magnetisation reversal by domain wall motions rather than by coherent rotation. So, by carefully choosing the biasing field strength, a good compromise between linearity and sensitivity can be achieved.

If there are magnetic particles above the sensor, like in Fig. 1a, and we apply a magnetic field parallel to the film structure, the PHE voltage will be affected. The stray field generated by the magnetic beads will change the effective field inside of the sensor.

We present some results regarding micromagnetic modelling of a PHE sensor using a more complex structure, than presented in Fig. 5a, which consists in a number of single domains of Permalloy, 10 nm thick and 95 nm each side. The distance between the adjacent domains is $d = 5$ nm which is equivalent with an inter-grain spacing (se also Fig. 1c). These elements are placed to form a disk. The conductive stripe which produces the biasing field is also considered. Figure 7a presents an image taken from SimulMag program during the micromagnetic simulations made on this sensor with 4 superparamagnetic grains placed above his surface at a distance of 200 nm. For a polarisation of 100 Oe, we performed micromagnetic simulations to obtain the response of the PHE sensor as depicted in Fig. 7a. The results, Fig. 7b, show the possibility to detect a single bead of magnetite, 200 nm in diameter with $M_S = 110$ emu/cm. The fields, H_b and H_{appl}, are applied like in Fig. 5a.

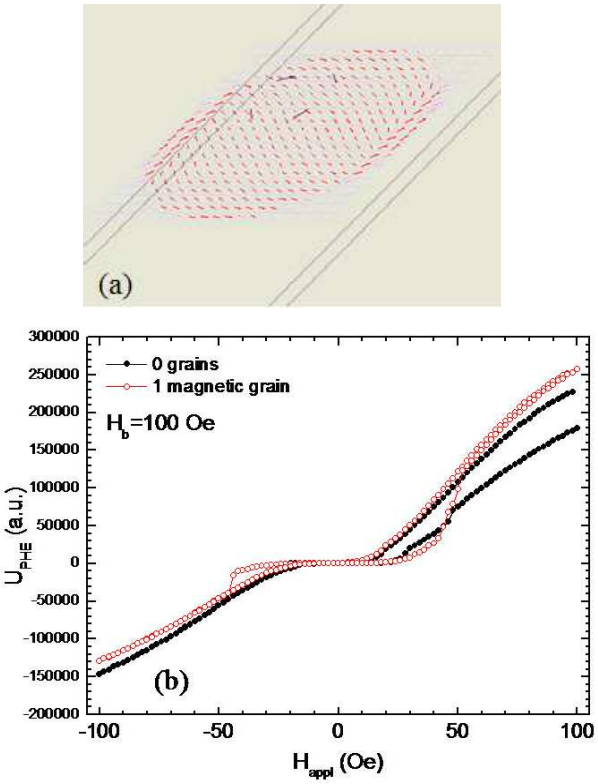

Fig. 7. (a) Micromagnetic simulations on magnetic moments orientations on a Permalloy disk biased at 100 Oe using a conductive band of Cu placed beneath the sensor; 4 sppm beads, 200 nm, are placed above the centre of the sensor at a distance of 200 nm. (b) The simulated response of the PHE sensor in the presence of a single bead of magnetite.

The appearance of the plateau at low fields, Fig. 7b, is the result of two factors: the sensor sensitivity and the nanoparticle fields. When the applied field H decreases from saturating values, the field of the nanoparticles decreases with the decreasing H. So, the perturbation on the PHE sensor due to the nanoparticle decreases. As it is expected, a net signal can be obtained in a field scan, as can be seen in Fig. 7b. The sppm bead is centred above the sensor' surface.

2.3. Manipulation of molecules by magnetic carriers using a simple circuit

Besides the detection of single markers and molecules, it is also possible to manipulate them on-chip. One example of the actuating and positioning of single markers is shown in Fig. 8 and is based on the high magnetic field gradient which is produced by this V shape configuration through which a current is flowing.

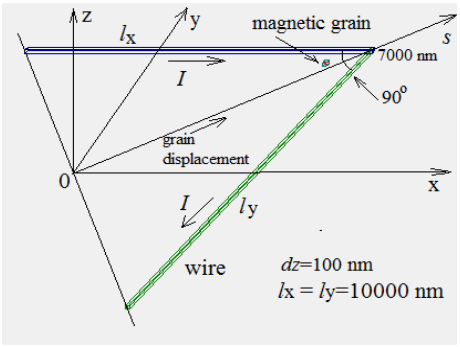

Fig. 8. The design of a circuit for exact positioning of magnetic markers made with SimulMag.

In our model, a current of 20 mA flows through the conducting line and creates the magnetic gradient field. The angle between the two wires is 90°. The superparamagnetic markers are used in an aqueous solution and are magnetized by the magnetic field generated by the conducting lines. The magnetized markers reorient and follow the gradient of the same magnetic field to a local maximum. If the particle is forced to move along Os axis, which is assumed to be a microchannel, the force which acts on this particle has the position dependence presented in Fig. 9. These results have been obtained by exploiting a special feature of the program SimulMag which returns the Ox, Oy and Oz field components in each point where the sppm particle is located. Our results are in good agreement with experimental data [1].

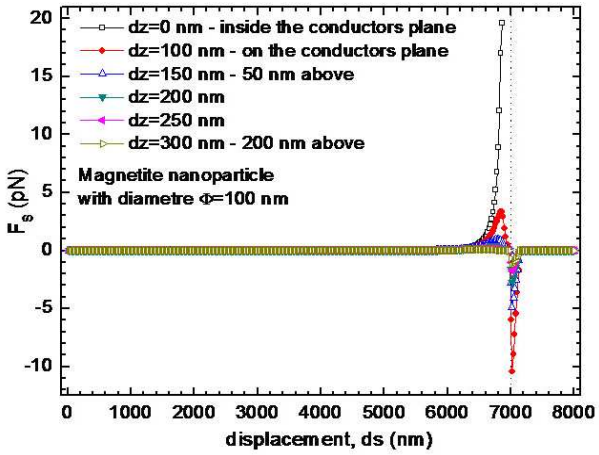

Fig. 9. The position dependence of the force directed over Os axis.

The sharp peaks show that it is possible to actuate and position with a very high precision the magnetic nanoparticles. The negative peak is obtained for displacements higher than 7000 nm and shows a returning force. Also there is a downward force over z axis. Obvious, these results can be extended to higher dimensions. To move

single beads to several defined positions on a sample surface, a different star-like line design can be used [1]. In combination with embedded magnetoresistive elements, the single markers, respectively biomolecules, can be detected on specific sensor sites.

3. Conclusions

We performed micromagnetic simulations regarding the GMR and PHE response of a sensor covered with magnetic beads used for biomedical applications. We found that a net signal can be obtained even for single bead detection. The simulations will be refined, especially for PHE sensors, in order to obtain more accurate results. Based on this concept PHE sensors will be developed and characterized for different field orientations. As we mentioned in introduction, the application of the magnetic field perpendicular to the film surface has the advantage to eliminate the needs of a second sensor used as a reference.

Finally, we showed the possibility to manipulate the magnetic nanoparticles using a simple design.

These results are useful in the designing process of a detection system used in lab-on-chip devices or for magnetic characterization of magnetite nanoparticles.

Acknowledgements. The research presented in this paper is supported by the Sectoral Operational Programme Human Resources Development (SOP HRD), financed from the European Social Fund and by the Romanian Government under the contract number POSDRU/89/1.5/S/63700.

References

[1] Brzeska M. et al., Journal of Biotechnology, **112**, 25 (2004).

[2] Baselt D.R. et al., Biosens. Bioelectron., **13**, pp. 731–739 (1998).

[3] Schotter J. et al., Biosens. Bioelectron., **19**, pp. 1149–1156 (2004).

[4] de Boer B.M. et al., Biosens. Bioelectron., **22**, pp. 2366–2370 (2007).

[5] Germano J., Martins V.C. et al., Sensors, **9**, pp. 4119–4137 (2009).

[6] Chuia K.M., Adeyeye A.O., Li M.-H., Journal of Magnetism and Magnetic Materials, **310**, e992–e993 (2007).

[7] Hung Tran Quang, Oh Sunjong, Jeong Jong-Ryul, Kim CheolGi, Sensors and Actuators A, **157**, pp. 42–46 (2010).

[8] Volmer M., Avram M., Journal of Magnetism and Magnetic Materials, **321**, p. 1683 (2009).

[9] Oti J.O., *PC Micromagnetic Simulator*, `http://math.nist.gov/oommf/contrib/simulmag/`

[10] Volmer M., Neamtu J., Physica B: Condensed Matter., **372**, pp. 198–201 (2006).

[11] Volmer M., Neamtu J., Physica B: Condensed Matter., **403**, pp. 350–353 (2008).

[12] She Sheng-Xian et al., Chin. Phys. Lett., **26**, pp. 127503-1–127503-4 (2009).

[13] Li G. et al., Sensors and Actuators, **A 126**, pp. 98–106 (2006).